Synovial fluid proteome profile of surgical versus chemical induced osteoarthritis in rabbits

Sharifah Zakiah Syed Sulaiman [1] , **Wei Miao Tan** [1] , **Rozanaliza Radzi** [1] , **Intan Nur Fatiha Shafie** [1] , **Mokrish Ajat** [2] , **Rozaihan Mansor** [3] , **Suhaila Mohamed** [4] , **Norasfaliza Rahmad** [5] , **Angela Min Hwei Ng** [6] , **Seng Fong Lau** [Corresp. 1, 4]

[1] Department of Veterinary Clinical Studies, Universiti Putra Malaysia, Serdang, Selangor, Malaysia

[2] Department of Veterinary Preclinical Studies, Universiti Putra Malaysia, Serdang, Selangor, Malaysia

[3] Department of Farm and Exotic Animals Medicine and Surgery, Universiti Putra Malaysia, Serdang, Selangor, Malaysia

[4] Laboratory of Cancer Research UPM-MAKNA (CANRES), Institute of Bioscience, Universiti Putra Malaysia, Serdang, Selangor, Malaysia

[5] Agro Biotechnology Institute, Universiti Putra Malaysia, Serdang, Selangor, Malaysia

[6] Tissue Engineering Centre, Universiti Kebangsaan Malaysia Medical Centre, Cheras, Selangor, Malaysia

Corresponding Author: Seng Fong Lau
Email address: lausengfong@upm.edu.my

Background: Animal models are significant for understanding human osteoarthritis (OA). This study compared the synovial fluid proteomics changes in surgical and chemical induced OA models.

Methods: Thirty rabbits either had anterior cruciate ligament transection (ACLT) procedure or injected intra-articularly with monosodium iodoacetate (MIA, 8 mg) into the right knee. The joints were anatomically assessed, and the synovial fluid proteins analyzed using two-dimensional polyacrylamide gel electrophoresis (2DGE) and MALDI TOF/TOF mass spectrometry analysis at 4, 8 and 12 weeks. The proteins' upregulation and downregulation were compared with control healthy knees.

Results: Seven proteins (histidine-rich glycoprotein, beta-actin-like protein 2 isoform X1, retinol-binding protein-4, alpha-1-antiproteinase, gelsolin isoform, serotransferrin, immunoglobulin kappa-b4 chain-C-region) were significantly expressed by the surgical induction. They characterized cellular process (27%), organization of cellular components or biogenesis (27%), localization (27%) and biological regulation (18%), which related to synovitis, increased cellularity, and subsequently cartilage damage. Three proteins (apolipoprotein I-IV precursor, serpin peptidase inhibitor and haptoglobin precursor) were significantly modified by the chemical induction. They characterized stimulus responses (23%), immune responses (15%), biological regulations (15%), metabolism (15%), organization of cellular components or biogenesis (8%), cellular process (8%), biological adhesions (8%) and localization (8%), which related to chondrocytes glycolysis/death, neovascularization, subchondral bone necrosis/collapse and inflammation.

Conclusions: The surgical induced OA model showed a wider range of protein changes, which were most upregulated at week 12. The biological process proteins expressions showed the chemical induced joints had slower OA progression compared to surgical induced joints. The chemical induced OA joints showed early inflammatory changes, which later decreased.

SYNOVIAL FLUID PROTEOME PROFILE OF SURGICAL VERSUS CHEMICAL INDUCED OSTEOARTHRITIS IN RABBITS

[1]Sharifah Zakiah Syed Sulaiman, [1]Wei Miao Tan, [1]Rozanaliza Radzi, [1]Intan Nur Fatiha Shafie, [2]Mokrish Ajat, [3]Rozaihan Mansor, [4]Suhaila Mohamed, [5]Norasfaliza Rahmad, [6]Angela Ng Min Hwei, [1,4]Seng Fong Lau

[1]Department of Veterinary Clinical Studies, Faculty of Veterinary Medicine,

Universiti Putra Malaysia, 43400, UPM Serdang, Selangor;

[2]Department of Veterinary Preclinical Studies, Faculty of Veterinary Medicine,

Universiti Putra Malaysia, 43400, UPM Serdang, Selangor;

[3]Department of Farm and Exotic Animals Medicine and Surgery, Faculty of Veterinary Medicine,

Universiti Putra Malaysia, 43400, UPM Serdang, Selangor;

[4]Laboratory of Cancer Research UPM-MAKNA (CANRES), Institute of Bioscience,

Universiti Putra Malaysia, 43400, UPM Serdang, Selangor;

[5]Agro Biotechnology Institute,

43400, Serdang, Selangor;

[6]Tissue Engineering Centre,

Universiti Kebangsaan Malaysia Medical Centre, 56000, Cheras, Kuala Lumpur.

Corresponding Author:

Seng Fong Lau[1,4]

Universiti Putra Malaysia, UPM Serdang, Selangor, 43400, Malaysia

Email address: lausengfong@hotmail.com; lausengfong@upm.edu.my

32 **Abstract**

34 **Background:** Animal models are significant for understanding human osteoarthritis (OA). This

35 study compared the synovial fluid proteomics changes in surgical and chemical induced OA

36 models.

37 **Methods:** Thirty rabbits either had anterior cruciate ligament transection (ACLT) procedure or

38 injected intra-articularly with monosodium iodoacetate (MIA, 8 mg) into the right knee. The

39 joints were anatomically assessed, and the synovial fluid proteins analyzed using two-

40 dimensional polyacrylamide gel electrophoresis (2DGE) and MALDI TOF/TOF mass

41 spectrometry analysis at 4, 8 and 12 weeks. The proteins' upregulation and downregulation were

42 compared with control healthy knees.

43 **Results:** Seven proteins (histidine-rich glycoprotein, beta-actin-like protein 2 isoform X1,

44 retinol-binding protein-4, alpha-1-antiproteinase, gelsolin isoform, serotransferrin,

45 immunoglobulin kappa-b4 chain-C-region) were significantly expressed by the surgical

46 induction. They characterized cellular process (27%), organization of cellular components or

47 biogenesis (27%), localization (27%) and biological regulation (18%), which related to synovitis,

48 increased cellularity, and subsequently cartilage damage. Three proteins (apolipoprotein I-IV

49 precursor, serpin peptidase inhibitor and haptoglobin precursor) were significantly modified by

50 the chemical induction. They characterized stimulus responses (23%), immune responses (15%),

51 biological regulations (15%), metabolism (15%), organization of cellular components or

52 biogenesis (8%), cellular process (8%), biological adhesions (8%) and localization (8%), which

53 related to chondrocytes glycolysis/death, neovascularization, subchondral bone necrosis/collapse

54 and inflammation.

55 **Conclusions:** The surgical induced OA model showed a wider range of protein changes, which

56 were most upregulated at week 12. The biological process proteins expressions showed the

57 chemical induced joints had slower OA progression compared to surgical induced joints. The

58 chemical induced OA joints showed early inflammatory changes, which later decreased.

59

60

61

62

63

INTRODUCTION

64

65   Osteoarthritis (OA) is a joint degeneration disease caused by the imbalance between

66   cartilage degradation and synthesis, commonly due to aging. OA symptoms include joint pain,

67   inflammation, morning stiffness, and decreased physical function, especially in the knee and hip.

68   OA is characterized by deterioration of cartilage, formation of osteophyte and osteosclerosis,

69   degradation of subchondral bone and tendons, inflammation of the synovium tissue, perforation

70   of the trabecular plate, loss of trabecular bone and bone cysts (Burr & Gallant, 2012; Li et al.,

71   2013).

72   OA includes cartilage disorder and subchondral bone deterioration (Burr & Gallant,

73   2012; Goldring & Goldring, 2016). Articular cartilage degradation involves overexpression of

74   matrix catabolic enzymes, inflammation, oxidative stress, and deterioration of proteoglycan and

75   collagen matrix. Around 9.6% of males and 18% of females exceeding 60 years of age are

76   impacted by OA (World Health Organization, 2013), resulting in reduced quality of life and

77   productivity as well as an increased economic burden or medical cost (Salter et al., 2014).

78   Current therapies, which include physiotherapy, orthopedic aids (orthoses), drugs, and surgery

79   have limited efficacy. Pharmacological treatment has been limited due to adverse effects on

80   cartilage (Huskisson et al., 1995) and gastrointestinal tract (Davies et al., 1997), whereas surgical

81   intervention possesses many risks such as infection, blood clot and longer recovery rate.

82   Animal models used in pre-clinical OA research are classified into spontaneous and

83   induced OA, further subcategorized into surgically or chemically induced OA models. Surgical

84   OA induction modifies the joint strain/stress, leading to joint instability and damage. The

85   anterior cruciate ligament transection (ACLT) is the most common method for surgical induced

86   OA, entailing subchondral bone destruction and resulting in drastic cartilage changes (Lelovas,

87   2014). ACLT causes joint destabilization followed by post-traumatic osteoarthritis and

88   reproduces the articular cartilage degradation after ACL injury (Piskin et al., 2007), or blunt

89   trauma to cartilage, menisci, and subchondral bone (Teeple et al., 2013). The surgical model

90   effectively yields a rapid OA progression; hence, it is convenient for short-term research but not

91   for studies on early OA (Kuyinu et al., 2016). ACLT also causes changes in cell morphology and

92   tissue equilibrium, especially in the femoral condyle cartilage (Buckwalter et al., 2005). For

93   chemical induced OA, monosodium iodoacetate (MIA) is most commonly used (Guingamp et

94   al., 1997; Takahashi et al., 2017). MIA suppresses the glyceraldehyde-3-dehydrogenase activity

95   required for glycolysis in chondrocytes, resulting in apoptosis, cartilage degradation,

96   proteoglycan loss, functional joint impairment and subchondral bone lesions (Pitcher et al., 2016;

97   Xie et al., 2012), similar to human OA.

98   Previous reports compared bone changes, histology, biochemistry and biomechanics of

99   surgical versus chemical induced OA (Naveen et al., 2013) and concluded that chemical induced

100   OA mimicked human OA. Each of the induced OA models has its own advantages, and no single

101   model is considered the gold standard in assessing OA.

102   To the best of our knowledge, the synovial proteomic profiles between the two induced

103   models have not been compared yet. This study analyses the proteome profiles of synovial fluids

104   at different stages of surgical or chemical induced OA in rabbits, to provide further insights on

105   the pathophysiology of OA and pave the road for future applications.

106   **METHODS**

107   **Animals**

108   Thirty male New Zealand white rabbits (A-Sapphire Enterprise, Malaysia) aged 8–9

109   months and weighing 1.8–2.0 kg were placed in Animal Research Facility, Faculty of Veterinary

110   Medicine, Universiti Putra Malaysia. Each rabbit was kept in an individual stainless-steel cage at

111   22-25°C, under a 12hr/12hr light/dark cycle with 50-60% relative humidity. Rabbits were fed

112   with commercial rabbit pellets (Penternakan Hong Lee Sdn. Bhd., Malaysia) and given fresh

113   water ad libitum. The rabbits were acclimatized for one week prior to OA induction. Approval

114   by the Institutional Animal Care and Use Committee (IACUC), Universiti Putra Malaysia was

115   obtained for the experimental protocol (UPM/IACUC/AUP-R034). The rabbits were randomly

116   grouped into surgically induced OA rabbits and chemically induced OA rabbits, with 15

117   individuals in each group. Rabbits were further subdivided into week 4, week 8 and week 12

118   time groups with 5 individuals in each group. OA was induced at the right knees of the animals,

119   and the contralateral joint was used as a healthy control.

120

121

Preparation of animal model of surgically induced and chemically induced osteoarthritis

122

123   Anterior cruciate ligament transection (ACLT) was done for surgically induced OA
124 group on the right stifle with a scalpel, under surgically sterile conditions, as described by
125 Vignon et al (1987). The animals were anesthetized with Zoletil® (Virbac, Australia) at 3mg/kg
126 via intramuscular route and maintained with isoflurane (3%) (Piramal Healthcare, India). In
127 order to expose the anterior cruciate ligament, medial patella dislocation was performed by
128 lateral parapatellar arthrotomy approach with the stifle joint being fully flexed. Once visualized,
129 irrigation with sterile saline was made onto the stifle joint. Subsequently, using 4-0
130 polydioxanone suture, closure of the joint capsule and subcutaneous tissue was done. Skin
131 closure was done using 3-0 nylon suture. Tramadol (Duopharma, Malaysia) 2mg/kg was given
132 twice daily for three days as painkiller. The animals were caged with unrestricted movement
133 until anaesthetic recovery.

134   The OA chemical induction was administered with 0.32 ml of 25mg/ml monosodium
135 iodoacetate (MIA) (Sigma-Aldrich, USA) dissolved in saline, injected into the intraarticular
136 space of the stifle joint, under general anaesthesia (Zoletil®) at 2mg/kg via intramuscular route.

Euthanization and sample collection

137

138   Rabbits were visually inspected for any clinical signs, such as weight loss or immobility.
139 In each group, rabbits were subdivided into week 4, week 8 and week 12 time groups. Because
140 both joint amputations were required to collect the samples, rabbits were euthanized following
141 the experiment with 120 mg/kg pentobarbital sodium (Vetoquinol, France) to avoid suffering
142 caused by risk of infection and also immobilization. Knee joints were removed and immediately
143 fixed in 10% buffered formalin (Sigma-Aldrich, USA). After 24 hours, the muscle and tissue
144 surrounding the femur and tibia were removed carefully to avoid damaging the cartilage surface.
145 The proximal femur and distal tibia were placed in 10% buffered formalin. Medial and lateral
146 femoral condyle and tibial plateau of left and right stifle joints were photographed by P7000
147 digital camera (Nikon, Japan) at macro setting. They were examined for gross morphological
148 changes, including erosions at the medial and lateral articular cartilage surfaces. Synovial fluids
149 were collected via arthrocentesis, placed in a 1.5 ml microcentrifuge tube and stored immediately
150 at -80°C until subsequent analysis.

Histology

Bones from harvested joint were decalcified immediately fixed in 10% buffered formalin (Sigma-Aldrich, USA) and were decalcified with 10% formic acid (Nacalai Tesque, Japan) for 10 days. The femur and tibia were cut at a dorsal plane. Samples were dehydrated in a series of immersion in alcohol using Leica TP1020 Semi-enclosed Benchtop Tissue Processor (Leica Biosystem, Germany). Next, the samples were embedded in paraffin using Leica EG1150H and EG11559 Modular Tissue Embedding Center (Leica Biosystems, Germany) and sliced at 5 μm using Reichert-Jung 2045 Multicut Rotary Microtome (Leica Biosystems, Germany) and mounted on glass slides. Prior to staining, the slides were deparaffinized and hydrated using distilled water. Next, they were stained using Fast Green (FCF) solution for five minutes and rinsed with 1% acetic acid before being stained using 0.1% Safranin-O solution for five minutes. The slides were dehydrated and cleared with 95% ethyl alcohol and absolute ethyl alcohol, alternately at two minutes each for two times. The slides were then observed under microscope (Motic, China) under 20x magnification and scored independently by two blinded observers. The changes of articular cartilage were scored using OARSI Scoring System (Pritzker et al., 2006). Histological evaluation of subchondral bone was done by measuring the percentage of bone volume over tissue volume (BV/TV). The measurement was done according to Nagira et al. (2020). In brief, the compartments of osteochondral units were defined, including cancellous bone (Cn.B), bone marrow (BM) and trabecular bone (Tb.B)(Figure 1). The calculation of BV/TV was done as follows: Bone volume (BV/TV, %) = (Cn.B region - BM regions)*/Cn.B region × 100, (*Cn.B region - BM regions = Tb.B regions) (Figure 1). Calculations were done using ImageJ with bone histomorphometry method.

Figure 1: Definition of tissue compartment in subchondral bone. White square dotted line, cancellous bone (Cn.B), yellow round dotted line, bone marrow (BM). Calculation of BV/TV: Bone volume (BV/TV, %) = (Cn.B region – BM regions)*/Cn.B region ×100, * Cn.B region – BM regions = Tb.B regions.

Statistical analysis

Sample size estimation using power analysis was performed before conducting the experiment, which was based on prior work that detected 23 significantly differentially

182 expressed proteins between OA induction group and control group (Luo et al., 2018). A sample

183 size of seven rabbits per group were determined (α = 0.05, power > 80%). However, in view of

184 the large sample size, sample size of 5 rabbits per group was chosen as suggested by the Animal

185 Research Committee. Power analysis was done using G*Power software (Faul et al., 2007).

186 Articular cartilage scoring data were tabulated as median and statistical comparisons for scoring

187 between groups were analysed using the Kruskal-Wallis (K-W) non-parametric ANOVA and

188 followed up with Dunn's multiple comparison tests. BV/TV value of subchondral bone

189 evaluation were analysed using one-factor analysis of variance (ANOVA) and multiple

190 comparison among groups were analysed using Tukey's HSD post hoc test. All analysis were

191 done using Graphpad Prism 7 (Graphpad Software, USA). The level of significance was at

192 α=0.05.

193 **Protein precipitation from synovial fluid**

194 Proteins from synovial fluid were precipitated using modified TCA/Acetone precipitation

195 method (Chen et al., 2005). Before protein precipitation, synovial fluid samples were centrifuged

196 at 3000 x g at ambient temperature for 10 minutes to remove cells and cellular debris. The

197 synovial fluid samples were pooled for each group and precipitated with cold 10%

198 trichloroacetic acid (TCA) (Chemiz, Malaysia) in 1:4 ratio inside a microcentrifuge tube.

199 Samples were kept for 60 minutes in a -20 °C chiller, before centrifugation at 12 000 x g for 60

200 minutes at 4 °C. The supernatant was removed without disrupting the protein pellet. Protein

201 pellets were washed three times with cold 100% acetone and centrifuged at 14 000 x g for 20

202 minutes, then the supernatant was removed. Finally, the microcentrifuge tube was inverted on the

203 C-fold tissue and air-dried for 30 seconds.

204 **Protein concentration estimation**

205 Protein pellets were resuspended and solubilized with rehydration buffer containing 7 M

206 urea, 2 M thiourea, 4 % CHAPS, and 0.002 % bromophenol blue. Protein concentration was

207 determined using the 2D Quant Kit (GE Healthcare, Sweden), following manufacturer's protocol.

208 A standard curve was obtained using 2 mg/ml Bovine serum albumin (BSA) stock solution. 500

209 µl precipitant was inserted into each tube, vortexed and incubated at ambient temperature for 2–3

210 minutes, then 500 µl co-precipitant was added. Tubes were then vortexed and centrifuged for 5

211   minutes at 10 000 x g and supernatant discarded. The tubes were centrifuged again. The residual

212   supernatant was decanted. Copper solution (100 µl) and distilled water (400 µl) were added to

213   each tube, and precipitated protein was dissolved by vortexing. The working reagent (1 ml) was

214   added to each tube and mixed by inversion instantaneously. Absorbance was measured using

215   Cary®50 UV-Vis spectrometer at 480 nm (Varian Inc., United States).

216   **Isoelectric focusing**

217   Synovial fluid protein (250 µg) was rehydrated overnight using 13 cm immobilized pH

218   gradient strips pH 3–10 ImmobilineTM DryStrip gels (IPG) (GE Healthcare, Sweden). The

219   samples were focused with a low starting voltage followed by a voltage gradient of 15 000 to 20

220   000 V, with a 50 mA strip limiting current. Strips were stored at -80 ° C until further analysis.

221   **Two-dimensional gel electrophoresis (2DGE)**

222   For 2DGE, strips were first equilibrated for 15 minutes with 50 mg dithiothreitol (DTT)

223   in equilibrium solution (50 mM tris-HCl pH 8.8, 6 M urea, 30 % glycerol, 2 % SDS, 0.002 %

224   bromophenol blue) (GE Healthcare, Sweden), followed by 15 minutes alkylation using 125 mg

225   iodoacetamide (IAA) (GE Healthcare, Sweden) in equilibrium solution. The strips were

226   positioned on top of 12 % gradient slab polyacrylamide gels and secured with molten 0.5 %

227   agarose in running buffer (25 mM tris pH 8.3; 198 mM glycine; 0.1 percent w/v SDS) with a

228   drop of bromophenol blue. Gels were run at 140 V for 10 minutes, then at 200 V for 55–60

229   minutes using Ruby SE 600 system (GE Healthcare, Sweden). Gels were stained using colloidal

230   Coomassie R350 (GE Healthcare, Sweden) and destained using destaining solution (40 %

231   methanol, 7 % glacial acetic acid, 53 % distilled water).

232   Gel images were obtained using a GS-800TM Optimized Densitometer for intra-sample

233   and inter-sample variability evaluation (Bio-Rad Laboratories, US). The digitized images were

234   aligned and analyzed using Progenesis SameSpots software (Nonlinear Dynamics, Durham, NC).

235   According to manufacturer's instruction, spots were detected, matched and normalized.

236   Differential protein spots between control and induced models were determined using

237   normalized spots and compared with reference gel image. Fold difference and p-values were

238   calculated using one-way ANOVA. Threshold value was set at 1.5 fold change for upregulation

239   and downregulation with p≤0.05.

240 **Protein digestion and matrix-assisted laser desorption/ionization time of flight/time of flight**

241 **mass spectrometry (MALDI-TOF/TOF)**

242   Gels were rinsed twice using distilled water, and 2DGE spots were excised manually

243 under sterile conditions. Spots were digested in a two-day process. On day one, the excised gel

244 spots were washed with 150 μl of 100 mM ammonium bicarbonate (ABC) for 10 minutes and

245 vortexed. Following that, wash solution (50% acetonitrile in 100 mM ABC) was added twice, 5

246 minutes for each wash. This process was repeated until the gel dye was utterly destained.

247 Reduction solution (150 μl of 10 mM DTT in 100 mM ABC) was then added and gel spots were

248 incubated at 60 °C in water bath for 30 minutes. Alkylation solution (150 μl of 55 mM IAA in

249 100 mM ABC) was added before incubation in the dark for 20 minutes. The solution was

250 removed, and wash solution was added twice, 20 minutes for each wash. Next, 50 μl of 100%

251 acetonitrile was added and incubated at ambient temperature for 15 minutes. Gel spots were then

252 vacuum-dried using ScanVac (Labogene, Denmark) for 1 hour. Finally, 25 μl of 7 ng/μl trypsin

253 solution were added, before incubation overnight at 30 ˚C. On the next day, 25 μl of 50%

254 acetonitrile were added and gel spots were incubated for 15 minutes at ambient temperature.

255 After centrifugation at 14 000 x g, supernatant samples were collected and transferred to new

256 tubes. Then, 20 μl of 100% acetonitrile were added before incubation for 15 minutes. The

257 obtained solution was transferred into a new tube and the peptide was vacuum-dried and

258 resuspended with 5 μl–10 μl of 0.1% trifluoroacetic acid. The digested protein sample underwent

259 desalting and concentration using μZipTipC18 pipette tips (Millipore, Bedford, MA, USA).

260 Protein samples were then analyzed using ultraflextreme MALDI-TOF/TOF mass spectrometer

261 (Bruker, Bremen, Germany). Peptide-matrix compounds were loaded using the dried droplet

262 technique on the instrument target plate. The used matrix compound was α-cyano-4-

263 hydroxycinnamic acid (CHCA) (Bruker, Bremen, Germany). Samples were analyzed with

264 MASCOT version 3.5 (Matrix science, USA) using the MASCOT search engine against the

265 sequence of *Oryctolagus cuniculus* species in the NCBInr database. Samples with p≤0.05 were

266 accepted as significant.

267

268 **RESULTS**

269 **General condition of rabbit models**

270   Compared to the chemically induced OA joints, the joint effusion development in the

271   surgically induced OA joints showed a more severe time-dependent swelling and warmth. Both

272   groups showed no clinical signs of pain, immobility or reduction in body weight and were

273   healthy prior to euthanization. The rabbits' average weight prior to euthanasia is 2.4 kg and

274   ranged from 1.8 kg–3.6 kg.

275   **Visual inspection of the joint and gross anatomy of the femoral condyle and tibial plateau**

276   The gross morphology of the femoral condyle and tibial plateau showed no significant

277   changes before week 4 and were similar to the control. The articular cartilage of the joints from

278   both induced OA groups was smooth and polished without any surface irregularities. OA

279   features such as surface erosions were observed on the femur and the tibia of both groups in

280   week 8. Erosions were more notable on the femur lateral condyle cartilage but had generalized

281   distribution on the tibia articular cartilage. The joints displayed similar significant osteoarthritic

282   features in both induced OA groups at week 12. Joints from surgically induced OA had more

283   apparent erosion on the medial condyle of femoral and tibial cartilages. In contrast, joints from

284   chemically induced OA showed evenly distributed erosions at the articular cartilage surface.

285   **Histopathological articular cartilage grading, subchondral bone evaluation and statistical**

286   **analysis**

287   Significant cartilage erosion was found in surgically induced and chemically induced OA

288   group whereas control group showed a normal chondrocytes distribution and smooth cartilage

289   surface in both femur and tibia. OARSI histopathology score was shown in Table 1 and Figure 2,

290   and representative histological images for femur and tibia was shown in Figure 3 and Figure 4.

291   For femur, in the surgically induced group, uneven articular surface and superficial fibrillation

292   were observed (Fig. 3B, 3C) at week 4 and week 8 after induction. Superficial zone fibrillation

293   was observed during week 12. Chemically induced group showed a more severe articular

294   cartilage changes indicated by cartilage erosion which was observed during week 8 and week 12

295   (Fig. 3G, 3H). For tibia, surgically induced group showed superficial fibrillation and

296   chondrocytes apoptosis indicated by empty chondrons during week 8. During week 12, deep

297   fibrillation and surface discontinuity was observed. Again, chemically induced group showed a

298   more severe changes with surface erosion presence during week 8 and week 12 (Fig. 4G, 4H).

299   Histopathological evaluation of subchondral bone recorded decreased BV/TV value in

300   surgically induced group for week 4 and week 8 in comparison with control (Fig. 5). At week 12,

301   BV/TV value in surgically induced group increased slightly compared to week 8. For chemically

302   induced group, BV/TV value decreased persistently from week 4 until week 12. The same

303   pattern was recorded for both induction groups for tibia bone.

304

305   **Table 1: OARSI histopathological grade of femur and tibia in the control, week 4, week 8 and week**

306   **12 for the surgically and chemically induced group**

307

308   **Figure 2: OARSI histopathological scores for (A) surgically induced femoral cartilage (B)**

309   **chemically induced femoral cartilage (C) surgically induced tibial cartilage (D) chemically induced**

310   **tibial cartilage.** Values are presented in median with 95% confidence interval (n=5). Significant

311   difference (Dunn's multiple comparisons, p<0.05) between column with the same letter within the

312   groups.

313

314   **Figure 3: Representative histology images of femoral articular cartilage. A-D: surgically induced**

315   **group. E-H: chemically induced group. Safranin-O/fast green stained with 20x magnification.**

316   Surgically induced group showed apoptosis indicated by empty chondrons (red arrow) during week 4 and

317   superficial fibrillation (red asterisk) during week 8. Chemically induced group showed surface erosion as

318   early as week 8 (red arrowhead).

319

320   **Figure 4: Representative histology images of tibial articular cartilage A-D: surgically induced**

321   **group. E-H: chemically induced group. Safranin-O/fast green stained with 20x magnification.**

322   During week 4, surgically induced group showed chondrocyte apoptosis (red arrow) and fibrillation (red

323   asterisk) during week 8. Cartilage erosion (red arrowhead) were present during week 12. For chemically

324   induced group, erosion can be observed during week 8 and week 12.

325

326   **Figure 5: Subchondral bone BV/TV values for (A) femur and (B) tibia in week 4, week 8 and week**

327   **12 for the control, surgically (ACLT) and chemically (MIA) induced group.** No significant difference

328   between groups were reported. The results are represented as mean (± SD).

329

330   **Evaluation of protein yield and two-dimensional gel electrophoresis analysis**

331   The precipitated protein concentrations from both induction groups ranged between 3.11–

332   19.9 µg/ml. The 2DGE gels showed that throughout OA progression protein expression profiles

333   are different from healthy control. The joints from surgically-induced OA displayed 28

334   significant matched spots (p≤0.05; fold change expression≥1.5) (Fig. 6A), whereas joints from

335   chemical induced OA displayed a total of 23 matched protein spots (p≤0.05; fold change

336   expression≥1.5) (Fig. 6B). The log normalized volume were calculated using SameSpot

337   software. The spots were then manually excised and identified using MALDI-TOF/TOF.

338   **Figure 6: Representative 2DGE (pI 3-10) image for rabbit synovial fluid in (A) surgically induced**

339   **group and (B) chemically induced group after staining with colloidal Coomassie stain.** Gels from

340   respective groups were scanned and analyzed with Progenesis SameSpot software and protein spots

341   (circled in red) were selected to be picked.

342

343   **Identification of proteins spots**

344   Twenty eight and 11 non-redundant proteins were identified from joints with surgical

345   induced and chemical induced OA, respectively. However, only seven proteins from surgical

346   induced OA joints and three proteins from the chemical induced OA joints have significantly

347   different (p≤0.05) fold-change expressions (≥1.5) when analyzed as log normalized volume

348   (Table 2).

349   **Table 2: List of proteins and their log normalized volume for control, week 4, week 8 and week 12**

350   **for both induction groups.** The results are represented as mean (± SD).

351

352   The proteins were classified by their biological process functions (Table 3). In the

353   surgically induced OA joints, proteins were characteristics of cellular process (27%),

354   organization of cellular components or biogenesis (27%), localization (27%) and biological

355   regulation (18%). For chemically induced OA joints, proteins were involved in stimulus

356   responses (23%), immune responses (15%), biological regulations (15%), metabolism (15%),

357   organization of cellular components or biogenesis (8%), cellular process (8%), biological

358   adhesions (8%) and localization (8%).

359   **Table 3: Characterization of proteins according to biological group for surgically and chemically**

360   **induced group.**

361 **DISCUSSION**

362   The effusion developments in the surgically induced OA joints were observed as early as

363 week 4 and increased significantly until week 12. Other reports on *in vivo* OA rabbit models

364 detected severe joint effusion 2 weeks post-surgery, which grew prominent at week 8. The

365 effusion in the surgically induced OA joints was more severe compared to the chemically

366 induced OA joints, probably indicating greater post-operative inflammation severity (Bouchgua

367 et al., 2009).

368   The gross morphology suggested that the OA damage in both groups was only manifest

369 after 8 weeks post-induction. In surgically induced OA, joint lesions were more prominent on the

370 medial condyle area, which is similar in humans, where the medial compartment is the most

371 commonly affected. This relates to the meniscus functions, as the medial meniscus is the more

372 important attachment for tibia movement at the knee (Campos et al., 2013). Thus, the ACLT

373 model most effectively mimics human post-traumatic osteoarthritis (PTOA). Histological

374 assessment of cartilage and subchondral bone is accepted as a gold standard in assessing and

375 monitoring OA progression in animal models. This assessment can be used to observe different

376 stages of joint degeneration (Rutgers et al., 2010).

377   Histological analysis revealed slight articular cartilage changes in surgically and

378 chemically induced (Man & Mologhianu, 2014) OA during week 4 which indicated initiation of

379 OA in both groups that may be pronounced over time. This is in line with previous report in

380 which ACLT model in rabbits showed slower lesion progression between 3 and 6 weeks and the

381 intensity of the lesion increases 6 weeks post-induction (Campos et al., 2013). During week 8

382 and week 12, more severe changes were observed in chemically induced group based on higher

383 histological scoring. Similarly, previous study detected obvious degenerative changes in the

384 cartilage as early as six to ten weeks after monosodium iodoacetate induction (Mohan et al.,

385 2011). Subchondral bone histopathological evaluation in surgically induced group showed

386 increased BV/TV values during week 12, suggesting the occurrence of bone remodeling

387 indicating higher OA progression (Fell et al., 2019). As for chemically induced group,

388 continuous decline in BV/TV throughout 12 weeks may be due to less loading of induced knee

389 which triggered weight distribution alterations (Guingamp et al., 1997).

390   Induction using monosodium iodoacetate will lead to chondrocytes apoptosis that will

391   first cause changes in morphological and histological features of articular cartilage before

392   changes in subchondral bones (Naveen et al., 2013). On the other hand, surgical induction using

393   ACLT method will cause destabilization of the joint and increased load at subchondral bone.

394   Osteoclasts' activity will increase and induced subchondral bone loss (Botter et al., 2009) and

395   subsequently bone remodeling at later stages. Therefore, subchondral bone resorption is the

396   initiating factor for articular cartilage degradation in surgically induced group and it can be

397   concluded that changes in the bone preceded changes in the articular cartilage in ACLT

398   induction (Yang et al., 2020).

399   The proteome profiles revealed four similar proteins detected in both groups: histidine-

400   rich glycoprotein (HRG), serotransferrin, alpha-1-antiproteinase and immunoglobulin. Only

401   HRG, serotransferin and alpha-1-antiproteinase expressions were significantly changed in the

402   surgically induced OA joints. Immunoglobulin is one of the most highly expressed proteins, and

403   its presence in both groups was expected since no depletion kit was used in this study. HRG,

404   detected in both groups, is a multifunctional plasma protein interacting with the immune system.

405   Previous studies showed that HRG binds strongly to some complementary proteins such as c4b

406   binding protein, C1q, and factor H, and is one of the most present proteins in rheumatoid arthritis

407   patients' synovial fluid and plasma (Manderson et al., 2009). However, the role of HRG in OA is

408   still unclear.

409   An upregulation of most identified proteins was observed in joints from surgically and

410   chemically induced OA. Nevertheless, surgically induced OA displayed slight downregulation of

411   alpha-1-antiproteinase protein, an acute-phase protein that protects tissue from uncontrolled

412   proteolysis damage and is upregulated by pro-inflammatory interleukin-6 (Ucar et al., 2007).

413   Such decrease indicates that inflammation and chondroprotection loss started at week 4 in the

414   surgically induced OA model.

415   The retinol-binding protein 4 (RBP-4) was more upregulated in week 4 compared to

416   week 8 and week 12. It belongs to the lipocalin family and is a blood retinol carrier positively

417   correlated with the collagen degrading matrix metalloproteinases (MMPs) MMP-1 and MMP-13

418   (Scotece et al., 2018). MMP-13 was released in response to mechanical injury or joint

419 destabilization (Rose & Kooyman, 2016), so this could explain RBP-4 expression in surgically
420 induced OA joints.

421   In chemically induced OA joints, apolipoprotein I-IV precursor and serpin peptidase
422 inhibitor proteins were most upregulated at week 4 compared to week 8 and week 12.
423 Apolipoprotein is a pro-inflammatory acute-phase protein involved in lipid and cholesterol
424 metabolism, found to be upregulated synovial fluids of OA patients (Nguyen et al., 2017).
425 Apolipoprotein induces IL-6 expressions in human primary chondrocytes (De Seny et al., 2015).
426 Serpin peptidase inhibitor inhibits serine proteases and MMPs regulation, aggrecanase plasmin,
427 angiogenesis activity, tissue mitogens and inflammatory leukocyte proteases (Gobezie et al.,
428 2007) in OA. These protein control processes such as inflammation and coagulation. The
429 upregulation of apolipoprotein suggested that joint inflammation occurs early at week 4 post-
430 induction. This consequently caused increased serpin peptidase inhibitor expression, which is
431 negative feedback for MMP regulation following OA-related joint inflammation.

432   During week 8, downregulation of beta-actin-like protein-2 isoform X1 and RBP-4 was
433 observed in surgical induced OA joints compared to the control group. Upregulation during week
434 4 followed by downregulation during week 8 indicated that OA progression was ongoing. Beta-
435 actin-like protein 2 isoform X1 is a highly conserved protein responsible for cell motility,
436 structure and integrity. Beta-actin-like protein 2 isoform X1 was most upregulated in the femur
437 lateral secretome of early OA patients (Stenberg et al., 2013) and was also identified in synovial
438 fluid of OA patients (Gobezie et al., 2007).

439   In chemically induced OA joints, the haptoglobin precursor was highly upregulated.
440 Haptoglobin has immunomodulatory effects and reduces hemolysis-associated oxidative damage
441 by binding with free hemoglobin (Cray et al., 2009). The upregulation of haptoglobin precursor
442 indicated that OA progressed from week 4 and persisted until week 8. A previous study reported
443 haptoglobin expression was reduced as much as 70% in early shoulder OA patients (Wanner et
444 al., 2013). The increased haptoglobin level in advanced OA is due to later upstream cytokine
445 release (Liao et al., 2015).

446   In the surgically induced OA joints, the strongest upregulation of gelsolin and
447 serotransferrin occurs at week 12, indicating advanced stage OA. Gelsolin is a major
448 extracellular actin scavenging system component and a novel MMP-14 substrate, as shown in a

449 previous study that demonstrates the cleavage of plasma gelsolin by MMP-14 (Park et al., 2006).

450 MMP-14 can activate MMP-2 and MMP-13, involved in tissue turnover and upregulated in

451 diseased state (Rose & Kooyman, 2016). Gelsolin was decreased in rheumatoid arthritis patients

452 (Osborn et al., 2008) but increased in OA individuals (Mateos et al., 2012), where it is

453 considered a putative biomarker. Thus, gelsolin upregulation in surgically induced OA joints

454 from the early stage until week 12 indicates rapid disease progression because of MMP-14

455 activation.

456   Serotransferin upregulation was revealed in both types of OA joints. Serotransferin is

457 secreted from the liver and involved in iron transport from absorption sites, from heme

458 degradation to storage and utilization (Nylund et al., 2014). Serotransferin is a traditional acute-

459 phase protein that reflects increased OA and RA inflammatory conditions. In this study,

460 serotransferin levels are slightly downregulated in chemically induced joints and upregulated in

461 surgically induced joints. Other studies reported serotransferin downregulation in OA (Gharbi et

462 al., 2011; Nylund et al., 2014), which contradicts the results from our surgically induced model.

463 Serotransferrin was downregulated in early shoulder OA patients but upregulated by 50 % in late

464 OA patients (Wanner et al., 2013). This suggests that based on the protein expressed, surgically

465 induced OA progression may be more advanced at week 12 compared to chemically induced

466 OA.

467   Overall, surgically induced OA development occurred immediately after induction and

468 continuously progressed until the end of the experimental duration (week 12), when most of the

469 identified proteins were strongly upregulated. In chemically induced OA joints, the levels of the

470 identified proteins were highest during the initial stage of induction and lowered at the final

471 stage, suggesting that chemically induced OA develops rapidly during the initial stage but slows

472 down or partially recovers at the later stages, based on the results at the molecular level. In

473 surgically induced group, destabilization of the joint will trigger the release of proinflammatory

474 cytokines which subsequently activates acute phase response that were expressed by alpha-1-

475 antiproteinase protein. Concurrently, retinol binding protein-4 and gelsolin release activated

476 MMP related pathways. As for chemically induced group, increased articular cartilage

477 degradation will continue to release pro-inflammatory cytokines which in turn stimulated the

478 release of acute phase proteins such as haptoglobin precursor and apolipoprotein I-IV precursor

479   which involved in acute phase response. In addition, local response in the joint triggered a

480   negative feedback mechanism on the inflammatory response through the expression of serpin

481   peptidase inhibitor.

482   Surgically induced OA joints were associated with more cellular process changes.

483   Synovitis is characterized by increased cellularity and cartilage damage at the advanced OA

484   stages. Surgically induced OA mimics post-traumatic OA, which promotes angiogenesis (Liu et

485   al., 2019). In surgically induced OA joints, angiogenesis involves cellular biological migration,

486   growth and differentiation of endothelial cells, and organization of cellular components.

487   Apolipoprotein is the metalloproteinase substrate that modulates angiogenic responses

488   (Quintero-Fabián et al., 2019). Gelsolin, which is upregulated in surgically induced OA joints, is

489   an important regulator of cellular functions for osteoclasts motility and podosomes (cell adhesion

490   structures) formation (Silacci et al., 2004).

491   Chemically induced OA joints were associated with more diverse biological processes,

492   although this group has fewer significant protein changes. The most represented proteins were

493   involved in response to stimulus (23%) and in immune responses, biological regulation, and

494   metabolic process (15%). The MIA induction disrupts chondrocytes glycolysis by suppressing

495   glyceraldehyde-3-phosphatase dehydrogenase, subsequently causing mitochondrial pathway

496   chondrocyte apoptosis involving reactive oxygen species (ROS) production (Jiang et al., 2013),

497   neovascularization, necrosis and collapse of subchondral bone, as well as inflammation (Pitcher

498   et al., 2016). These processes involve changes in cell states and activities following a stimulus,

499   thus causing major upregulation of stimulus-response proteins. In chemical induced OA joints,

500   serpin peptidase inhibitor upregulation inactivates proteinase inhibition by ROS-associated

501   oxidative inactivation, which causes further joint inflammation (Jones et al., 1998). Haptoglobin

502   precursor and apolipoprotein are acute-phase proteins, released or activated in acute response

503   following defective chondrocyte metabolism (Sipe, 1995). In auto-inflammatory and non-auto-

504   inflammatory OA, immune regulation may be crucial for altering cell osmosis and inflammatory

505   response in periostitis, which is associated with osteophytes formation in OA (Lu et al., 2014).

506   This study indicates that surgically induced OA developed more rapidly compared to

507   chemically induced OA, based on the expressed biological process of proteins associated with

508   advanced stage OA. The choice of OA induction is depending on the type of study that will be

509   conducted, where surgically induced OA is suitable studies with a shorter time frame and

510   chemically induced OA is suited for studies that needed a longer duration.

511   Several limitations were noted in this study. The main limitation to this study is the small

512   numbers of animals in each group (n=5) for each time point which also reflected the absence of

513   sham control group. This is due to suggestion by Animal Care Committee as a consideration for

514   the welfare of the rabbits. While this may hampers a more robust conclusion, it does provide

515   significant preliminary data which may justify larger scale studies to be conducted. Also,

516   decision to use contralateral joint as control was to reduce the number of animals to be

517   sacrificed. In a study by Mustafy et al. (2018), contralateral joint can be accepted as a suitable

518   control model as they showed high degree of similarities, with no significant differences among

519   all evaluated mechanical, geometrical and morphological parameters. In addition, proteomics

520   analysis was done using synovial fluid which was in direct contact with primary tissues of each

521   joint. Hence, the results obtained for each joint would not completely correlated with each other

522   as proteins expressed in each joint were relatively different as synovial fluid reflected the

523   condition of each individual joint, showed focal changes in particular joints and therefore was

524   reliable in characterizing changes in control and experimental joints.

525   The limitations in using rabbit models is the difference in joint biomechanics and gait in

526   comparison with human, and structural difference in joint tissues (McCoy, 2015). However,

527   although the translatability of each animal models to human clinical conditions are different,

528   rabbit models are one of the widely used animal models as it is easily reproducible, low cost and

529   easier in handling.

530   Changes in meniscus and synovium can also be observed to further elucidate disease

531   progression as OA will cause degenerative changes in the meniscus by the loss of Type 1 and

532   Type II collagen. In addition, synovial macrophage which is originated from synovium will be

533   activated during inflammation process (Kuyinu et al., 2016). However, in this study, as synovial

534   fluid is originated from synovium that releases various cytokines and pro-inflammatory

535   mediators during disease progression (Danila, 2014), we would like to propose a non-invasive or

536   less invasive method to assess the progression of OA using synovial fluid. This method will

537   provide an early indication of OA development and intervention to stop or reduce further

538   degeneration of joint and can represent OA progression.

539   **CONCLUSIONS**

540   This study showed the surgical induced model showed a wider range of proteome profile

541   and had the highest upregulation of most proteins at week 12. On the other hand, chemically

542   induced joints have slower OA progression compared to surgically induced joints, based on the

543   biological process proteins expressed. The chemically induced joints showed inflammatory

544   changes at the early phase but had decreased expression at the later stages.

545   **ACKNOWLEDGEMENTS**

546   We would like to thank Dr. Murshidah Mohd Asri and Dr. Goh Soon Heng for helping during

547   the study.

548   **REFERENCES**

549   Botter SM, Glasson SS, Hopkins B, Clockaerts S, Weinans H, van Leeuwen JPTM, van Osch

550   GJVM. 2009. ADAMTS5-/- mice have less subchondral bone changes after induction of

551   osteoarthritis through surgical instability: implications for a link between cartilage and

552   subchondral bone changes. *Osteoarthritis and Cartilage*. DOI:

553   10.1016/j.joca.2008.09.018.

554   Bouchgua, M., Alexander, K., André d'Anjou, M., Girard, C. A., Carmel, E. N., Beauchamp, G.,

555   Richard, H., & Laverty, S. (2009). Use of routine clinical multimodality imaging in a

556   rabbit model of osteoarthritis - part I. *Osteoarthritis and Cartilage*.

557   https://doi.org/10.1016/j.joca.2008.06.017

558   Buckwalter, J. A., Mankin, H. J., & Grodzinsky, A. J. (2005). Articular cartilage and

559   osteoarthritis. In *Instructional course lectures*. https://doi.org/10.1136/ard.51.9.1028-a

560   Burr DB, Gallant MA (2012) Bone remodelling in osteoarthritis. *Nature Reviews Rheumatol*ogy.

561   Campos, W. N. S., Souza, M. A., Ruiz, T., Peres, T. P., Néspoli, P. B., Marques, A. T. C.,

562   Colodel, E. M., Souza, R. L. De, S, A. C. W. N., Souza, M. A., Ruiz, T., Peres, T. P.,

563   Néspoli, P. B., & Marques, A. T. C. (2013). *Experimental osteoarthritis in rabbits :*

564   *lesion progression 1*. *32*(3), 279–285.

565   Chen, Y. Y., Lin, S. Y., Yeh, Y. Y., Hsiao, H. H., Wu, C. Y., Chen, S. T., & Wang, A. H. J.
566   (2005). A modified protein precipitation procedure for efficient removal of albumin from
567   serum. *Electrophoresis*. https://doi.org/10.1002/elps.200410381

568   Cray, C., Zaias, J., & Altman, N. H. (2009). Acute phase response in animals: A review. In
569   *Comparative Medicine*.

570   Danila MI. 2014. Biology of Normal Joint and Evaluation of the Joint Including CLinical,
571   Imaging, and Pathologic Evaluation. In: *Pathobiology of Human Disease: A Dynamic*
572   *Encyclopedia of Disease Mechanisms*. DOI: 10.1016/B978-0-12-386456-7.04301-X.

573   Davies, N. M., Roøseth, A. G., Appleyard, C. B., Mcknight, W., Del Soldato, P., Calignano, A.,
574   Cirino, G., & Wallace, J. L. (1997). NO-naproxen vs. naproxen: Ulcerogenic, analgesic
575   and anti-inflammatory effects. *Alimentary Pharmacology and Therapeutics*.
576   https://doi.org/10.1046/j.1365-2036.1997.115286000.x

577   De Seny, D., Cobraiville, G., Charlier, E., Neuville, S., Lutteri, L., Goff, C. Le, Malaise, D.,
578   Malaise, O., Chapelle, J. P., Relic, B., & Malaise, M. G. (2015). Apolipoprotein-A1 as a
579   damage-associated molecular patterns protein in osteoarthritis: Ex vivo and in vitro pro-
580   inflammatory properties. *PLoS ONE*. https://doi.org/10.1371/journal.pone.0122904

581   Faul F, Erdfelder E, Lang AG, Buchner A. 2007. G*Power 3: A flexible statistical power
582   analysis program for the social, behavioral, and biomedical sciences. In: *Behavior*
583   *Research Methods*. DOI: 10.3758/BF03193146.

584   Fell NLA, Lawless BM, Cox SC, Cooke ME, Eisenstein NM, Shepherd DET, Espino DM. 2019.
585   The role of subchondral bone, and its histomorphology, on the dynamic viscoelasticity of
586   cartilage, bone and osteochondral cores. *Osteoarthritis and Cartilage*. DOI:
587   10.1016/j.joca.2018.12.006.

588   Gharbi, M., Deberg, M., & Henrotin, Y. (2011). Application for proteomic techniques in
589   studying osteoarthritis: A review. *Frontiers in Physiology*.
590   https://doi.org/10.3389/fphys.2011.00090

591 Gobezie, R., Kho, A., Krastins, B., Sarracino, D. A., Thornhill, T. S., Chase, M., Millett, P. J., &
592   Lee, D. M. (2007). High abundance synovial fluid proteome: Distinct profiles in health
593   and osteoarthritis. *Arthritis Research and Therapy*, *9*(2), 1–15.
594   https://doi.org/10.1186/ar2172

595 Goldring S. R., Goldring M. B. (2016) Changes in the osteochondral unit during osteoarthritis:
596   Structure, function and cartilage bone crosstalk. *Nature Reviews Rheumatology*.

597 Guingamp, C., Gegout-Pottie, P., Philippe, L., Terlain, B., Netter, P., & Gillet, P. (1997). Mono-
598   iodoacetate-induced experimental osteoarthritis: A dose-response study of loss of
599   mobility, morphology, and biochemistry. *Arthritis and Rheumatism*.
600   https://doi.org/10.1002/art.1780400917

601 Huskisson, E. C., Berry, H., Gishen, P., Jubb, R. W., & Whitehead, J. (1995). Effects of
602   antiinflammatory drugs on the progression of osteoarthritis of the knee. *Journal of*
603   *Rheumatology*.

604 Jiang, L., Li, L., Geng, C., Gong, D., Jiang, L., Ishikawa, N., Kajima, K., & Zhong, L. (2013).
605   Monosodium iodoacetate induces apoptosis via the mitochondrial pathway involving
606   ROS production and caspase activation in rat chondrocytes in vitro. *Journal of*
607   *Orthopaedic Research*. https://doi.org/10.1002/jor.22250

608 Jones HW, Bailey R, Zhang Z, Dunne KA, Blake DR, Cox NL, Morris CJ, Winyard PG. 1998.
609   Inactivation of antithrombin III in synovial fluid from patients with rheumatoid arthritis.
610   *Annals of the Rheumatic Diseases*. DOI: 10.1136/ard.57.3.162.

611 Kuyinu, E. L., Narayanan, G., Nair, L. S., & Laurencin, C. T. (2016). Animal models of
612   osteoarthritis: classification, update, and measurement of outcomes. *Journal of*
613   *Orthopaedic Surgery and Research*, *11*(1), 19. https://doi.org/10.1186/s13018-016-0346-
614   5

615 Lelovas, K. L. P. (2014). *Useful animal models for the research of osteoarthritis*. 263–271.
616   https://doi.org/10.1007/s00590-013-1205-2

617 Liao, W., Li, Z., Zhang, H., Li, J., Wang, K., & Yang, Y. (2015). Proteomic analysis of synovial
618   fluid as an analytical tool to detect candidate biomarkers for knee osteoarthritis.
619   *International Journal of Clinical and Experimental Pathology*.

620 Liu, C.-C., Lee, H.-C., Peng, Y.-S., Tseng, A. H., Wu, J.-L., Tsai, W.-Y., Wong, C.-S., & Su, L.-
621   J. (2019). Transcriptome Analysis Reveals Novel Genes Associated with Cartilage
622   Degeneration in Posttraumatic Osteoarthritis Progression. *CARTILAGE*.
623   https://doi.org/10.1177/1947603519847744

624 Lu, Q. Y., Han, Q. H., Li, X., Li, Z. C., Pan, Y. T., Liu, L., & Fu, Q. G. (2014). Analysis of
625   differentially expressed genes between rheumatoid arthritis and osteoarthritis based on
626   the gene co-expression network. *Molecular Medicine Reports*.
627   https://doi.org/10.3892/mmr.2014.2166

628 Luo Q, Qin X, Qiu Y, Hou L, Yang N. 2018. The change of synovial fluid proteome in rabbit
629   surgery-induced model of knee osteoarthritis. *American Journal of Translational
630   Research*.

631 Man G. S., Mologhianu G. 2014. Osteoarthritis pathogenesis - a complex process that involves
632   the entire joint. *Journal of medicine and life*.

633 Manderson, G. A., Martin, M., Önnerfjord, P., Saxne, T., Schmidtchen, A., Mollnes, T. E.,
634   Heinegård, D., & Blom, A. M. (2009). Interactions of histidine-rich glycoprotein with
635   immunoglobulins and proteins of the complement system. *Molecular Immunology*.
636   https://doi.org/10.1016/j.molimm.2009.07.011

637 Mateos, J., Lourido, L., Fernández-puente, P., Calamia, V., Fernández-lópez, C., Oreiro, N.,
638   Ruiz-romero, C., & Blanco, F. J. (2012). Differential protein profiling of synovial fluid
639   from rheumatoid arthritis and osteoarthritis patients using LC – MALDI TOF / TOF ☆.
640   *Journal of Proteomics*, *75*(10), 2869–2878. https://doi.org/10.1016/j.jprot.2011.12.042

641 McCoy AM. 2015. Animal Models of Osteoarthritis: Comparisons and Key Considerations.
642   Veterinary Pathology. DOI: 10.1177/0300985815588611.

643 Mohan G, Perilli E, Kuliwaba JS, Humphries JM, Parkinson IH, Fazzalari NL. 2011. Application
644   of in vivo micro-computed tomography in the temporal characterisation of subchondral
645   bone architecture in a rat model of low-dose monosodium iodoacetate-induced
646   osteoarthritis. *Arthritis Research and Therapy*. DOI: 10.1186/ar3543.

647 Mustafy T, Londono I, Villemure I. 2018. Can the contralateral limb be used as a control during
648   the growing period in a rodent model? *Medical Engineering and Physics*. DOI:
649   10.1016/j.medengphy.2018.04.013.

650 Nagira K, Ikuta Y, Shinohara M, Sanada Y, Omoto T, Kanaya H, Nakasa T, Ishikawa M, Adachi
651   N, Miyaki S, Lotz M. 2020. Histological scoring system for subchondral bone changes in
652   murine models of joint aging and osteoarthritis. *Scientific Reports*. DOI: 10.1038/s41598-
653   020-66979-7.

654 Naveen, S. V., Ahmad, R. E., Hui, W. J., Suhaeb, A. M., Murali, M. R., Shanmugam, R., &
655   Kamarul, T. (2013). Histology, glycosaminoglycan level and cartilage stiffness in
656   monoiodoacetate-induced osteoarthritis: Comparative analysis with anterior cruciate
657   ligament transection in rat model and human osteoarthritis. *International Journal of*
658   *Medical Sciences*. https://doi.org/10.7150/ijms.6964

659 Nguyen, L. T., Sharma, A. R., Chakraborty, C., Saibaba, B., Ahn, M. E., & Lee, S. S. (2017).
660   Review of prospects of biological fluid biomarkers in osteoarthritis. In *International*
661   *Journal of Molecular Sciences*. https://doi.org/10.3390/ijms18030601

662 Nylund, R., Lemola, E., Hartwig, S., Lehr, S., Acheva, A., Jahns, J., Hildebrandt, G., &
663   Lindholm, C. (2014). Profiling of low molecular weight proteins in plasma from locally
664   irradiated individuals. *Journal of Radiation Research*. https://doi.org/10.1093/jrr/rru007

665 Osborn, T. M., Verdrengh, M., Stossel, T. P., Tarkowski, A., & Bokarewa, M. (2008). *Research*
666   *article Decreased levels of the gelsolin plasma isoform in patients with rheumatoid*
667   *arthritis*. *10*(5), 1–9. https://doi.org/10.1186/ar2520

668   Park, S., Hwang, I. K., Kim, S. Y., & Lee, S. (2006). *Characterization of plasma gelsolin as a*
669   *substrate for matrix metalloproteinases*. 1192–1199.
670   https://doi.org/10.1002/pmic.200500402

671   Piskin, A., Gulbabar, M. Y., Tomak, Y., Gulman, B., Hokelek, M., Kerimoglu, S., Koksal, B.,
672   Alic, T., & Kabak, Y. B. (2007). Osteoarthritis models after anterior cruciate ligament
673   resection and medial meniscectomy in rats: A histological and immunohistochemical
674   study. *Saudi Medical Journal*.

675   Pitcher, T., Sousa-Valente, J., & Malcangio, M. (2016). The monoiodoacetate model of
676   osteoarthritis pain in the mouse. *Journal of Visualized Experiments*.
677   https://doi.org/10.3791/53746

678   Pritzker KPH, Gay S, Jimenez SA, Ostergaard K, Pelletier JP, Revell K, Salter D, van den Berg
679   WB. 2006. Osteoarthritis cartilage histopathology: Grading and staging. *Osteoarthritis*
680   *and Cartilage* 14:13–29. DOI: 10.1016/j.joca.2005.07.014.

681   Quintero-Fabián, S., Arreola, R., Becerril-Villanueva, E., Torres-Romero, J. C., Arana-Argáez,
682   V., Lara-Riegos, J., Ramírez-Camacho, M. A., & Alvarez-Sánchez, M. E. (2019). Role of
683   Matrix Metalloproteinases in Angiogenesis and Cancer. In *Frontiers in Oncology*.
684   https://doi.org/10.3389/fonc.2019.01370

685   Rose, B. J., & Kooyman, D. L. (2016). *A Tale of Two Joints : The Role of Matrix*
686   *Metalloproteases in Cartilage Biology*. *2016*. https://doi.org/10.1155/2016/4895050

687   Rutgers M, van Pelt MJP, Dhert WJA, Creemers LB, Saris DBF. 2010. Evaluation of
688   histological scoring systems for tissue-engineered, repaired and osteoarthritic cartilage.
689   *Osteoarthritis and Cartilage*. DOI: 10.1016/j.joca.2009.08.009.

690   Salter, D. M., Su, S. L., & Lee, H. S. (2014). Epidemiology and genetics of osteoarthritis. In
691   *Journal of Medical Sciences (Taiwan)*. https://doi.org/10.4103/1011-4564.147251

692   Scotece, M., Koskinen-Kolasa, A., Moilanen, T., Moilanen, E., & Vuolteenaho, K. (2018).
693   Novel adipokine associated with osteoarthritis: retinol binding protein 4 is produced by

694   cartilage and correlates withmatrix metalloproteinasesin osteoarthritis patients.

695   *Osteoarthritis and Cartilage*. https://doi.org/10.1016/j.joca.2018.02.276

696   Silacci, P., Mazzolai, L., Gauci, C., Stergiopulos, N., Yin, H. L., & Hayoz, D. (2004). Gelsolin

697   superfamily proteins: Key regulators of cellular functions. In *Cellular and Molecular Life*

698   *Sciences*. https://doi.org/10.1007/s00018-004-4225-6

699   Sipe, J. D. (1995). Acute-phase proteins in osteoarthritis. *Seminars in Arthritis and Rheumatism*.

700   https://doi.org/10.1016/S0049-0172(95)80020-4

701   Stenberg, J., Rüetschi, U., Skiöldebrand, E., Kärrholm, J., & Lindahl, A. (2013). Quantitative

702   proteomics reveals regulatory differences in the chondrocyte secretome from human

703   medial and lateral femoral condyles in osteoarthritic patients. *Proteome Science*.

704   https://doi.org/10.1186/1477-5956-11-43

705   Takahashi, I., Matsuzaki, T., & Hoso, M. (2017). Long-term histopathological developments in

706   knee-joint components in a rat model of osteoarthritis induced by monosodium

707   iodoacetate. *Journal of Physical Therapy Science*. https://doi.org/10.1589/jpts.29.590

708   Teeple, E., Jay, G. D., Elsaid, K. A., & Fleming, B. C. (2013). Animal models of osteoarthritis:

709   Challenges of model selection and analysis. In *AAPS Journal*.

710   https://doi.org/10.1208/s12248-013-9454-x.

711   Ucar, H. I., Tok, M., Atalar, E., Dogan, O. F., Oc, M., Farsak, B., Guvener, M., Yilmaz, M.,

712   Dogan, R., Demircin, M., & Pasaoglu, I. (2007). Predictive significance of plasma levels

713   of interleukin-6 and high-sensitivity C-reactive protein in atrial fibrillation after coronary

714   artery bypass surgery. *The Heart Surgery Forum*.

715   https://doi.org/10.1532/HSF98.20061175

716   Vignon, E., Bejui, J., Mathieu, P., Hartmann, J. D., Ville, G., Evreux, J. C., & Descotes, J.

717   (1987). Histological cartilage changes in a rabbit model of osteoarthritis. *Journal of*

718   *Rheumatology*.

719   Wanner, J. P., Subbaiah, R., Skomorovska-prokvolit, Y., Shishani, Y., Boilard, E., Mohan, S.,

720   Gillespie, R., Miyagi, M., & Gobezie, R. (2013). Proteomic profiling and functional

721   characterization of early and late shoulder osteoarthritis. *Arthritis Research & Therapy*,

722   *15*(6), 1. https://doi.org/10.1186/ar4369

723   World Health Organization. (2013). Chronic rheumatic conditions. In *Chronic deseases and*

724   *health promotion*.

725   Xie, L., Lin, A. S. P., Kundu, K., Levenston, M. E., Murthy, N., & Guldberg, R. E. (2012).

726   Quantitative imaging of cartilage and bone morphology, reactive oxygen species, and

727   vascularization in a rodent model of osteoarthritis. *Arthritis and Rheumatism*.

728   https://doi.org/10.1002/art.34370

729   Yang Y, Li P, Zhu S, Bi R. 2020. Comparison of early-stage changes of osteoarthritis in cartilage

730   and subchondral bone between two different rat models. *PeerJ*. DOI: 10.7717/peerj.8934.

731

732

733

OARSI histopathological grade of femur and tibia in the control, week 4, week 8 and week 12 for the surgically and chemically induced group.

	Control		Week 4		Week 8		Week 12	
	ACLT (median, range)	MIA (median, range)	ACLT (median, range)	MIA (median, range)	ACLT (median, range)	MIA (median, range)	ACLT (median, range)	MIA (median, range)
Femur	0	0	0 (0-1)	0.5 (0-1.5)	1 (0.5-2)	1.5 (1-1.5)	1 (0-2.5)	4.25 (2-5.5)
Tibia	0	0	0 (0)	1 (0.5-1)	0 (0-1)	3 (3-5)	2 (1.5-2.0)	5 (4.5-5.5)

List of proteins and their log normalized volume for control, week 4, week 8 and week 12 for both induction groups.

The results are represented as mean (± SD).

Surgically-induced group

Protein	Mean (± SD)			
	Control	**Week 4**	**Week 8**	**Week 12**
alpha-1-antiproteinase F precursor	5.11(±0.3)	5.1(±0.37)	5.5(±0.3)	5.35(±0.23)
histidine-rich glycoprotein	4.94 (±0.17)	5.03(±0.06)	5.1(±0.39)	5.41(±0.35)
retinol-binding protein 4	5.26(±0.18)	5.49(±0.12)	5.12(±0.35)	5.38(±0.42)
beta-actin-like protein 2 isoform X1	4.56(±0.28)	4.83(±0.21)	4.49(±0.38)	4.91(±0.04)
Full=Ig kappa-b4 chain C region	6.19(±0.41)	6.35(±0.23)	6.22(±0.07)	6.38(±0.09)
Serotransferrin	5.15(±0.2)	5.34(±0.3)	5.58(±0.51)	5.75(0.18)
Gelsolin isoform	4.94 (±0.17)	5.03(±0.05)	5.1(±0.39)	5.41(±0.35)

Chemically-induced group

Protein	Mean (± SD)			
	Control	**Week 4**	**Week 8**	**Week 12**
Serpin peptidase inhibitor	6.21 (±0.10)	6.47 (±0.08)	6.28 ± (0.22)	6.18 (±0.15)
Haptoglobin precursor	4.85 (±0.04)	5.05 (±0.13)	5.38 (±0.15)	5.07 (±0.27)
Apolipoprotein I-IV precursor	4.94 (±0.05)	5.45 (±0.20)	5.35 (±0.13)	5.21 (±0.11)

Characterization of proteins according to biological group for surgically and chemically induced group.

Surgically-induced group

Biological process	Percentage (%)
Cellular process	27
Cellular Component Organization & Biogenesis	27
Localization	27
Biological Regulation	18

Chemically-induced group

Biological process	Percentage (%)
Response to Stimulus	23
Immune System Response	15
Biological Regulation	15
Metabolic Process	15
Cellular Component Organization & Biogenesis	8
Cellular Process	8
Biological Adhesion	8
Localization	8

Figure 1

Definition of tissue compartment in subchondral bone.

White square dotted line, cancellous bone (Cn.B), yellow round dotted line, bone marrow (BM). Calculation of BV/TV: Bone volume (BV/TV, %) = (Cn.B region – BM regions)*/Cn.B region ×100, * Cn.B region – BM regions = Tb.B regions.
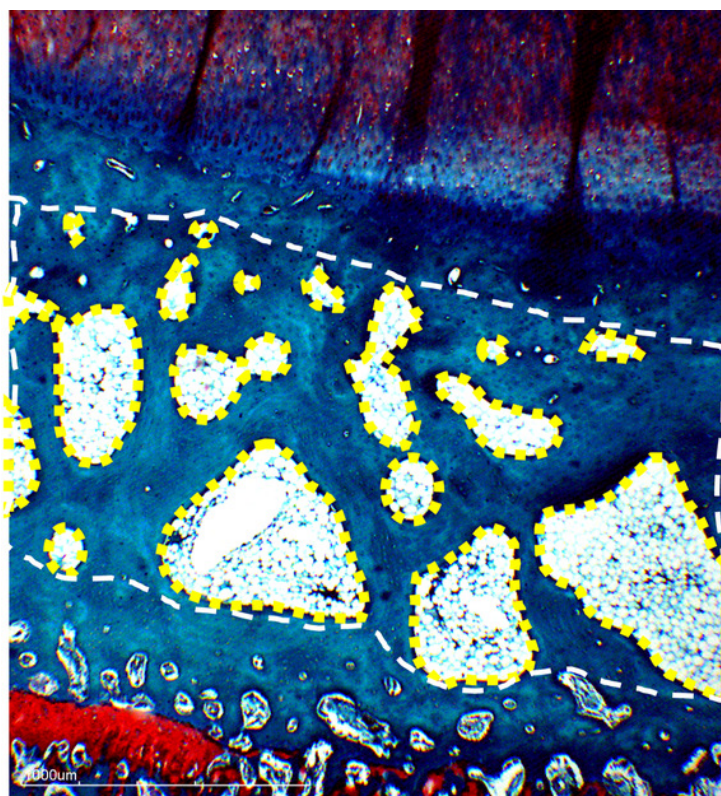
1. White square dotted line; cancellous bone (Cn.B)
2. Yellow round dotted line, bone marrow (BM)

Bone volume (BV/TV, %)
= Cn.B – BM / Cn.B x 100
= Trabecular bone (Tb.B) / Cn.B x 100

Figure 2

OARSI histopathological scores for (A) surgically induced femoral cartilage (B) chemically induced femoral cartilage (C) surgically induced tibial cartilage (D) chemically induced tibial cartilage.

Values are presented in median with 95% confidence interval (n=5). Significant difference (Dunn's multiple comparisons, p<0.05) between column with the same letter within the groups.
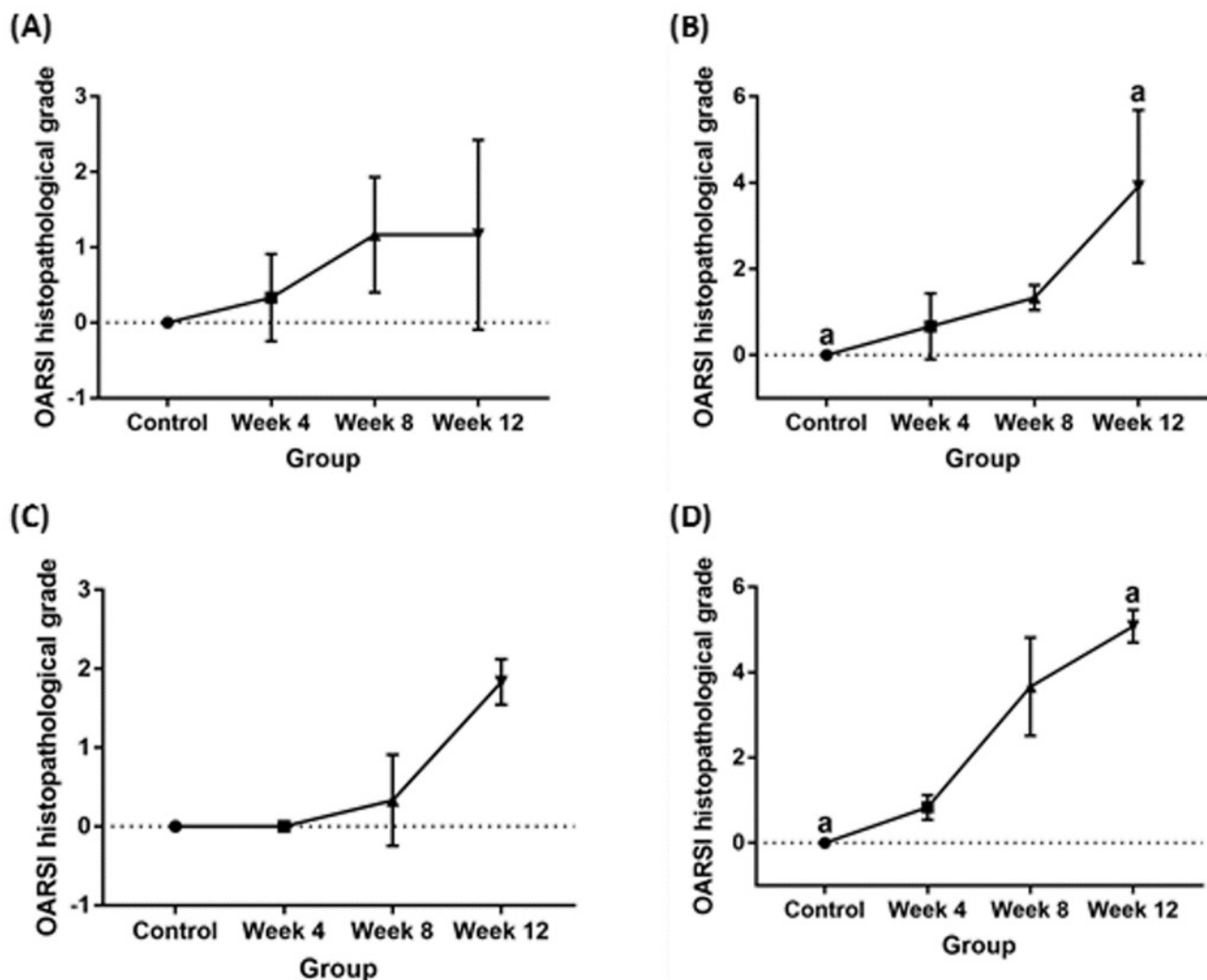
Figure 3

Representative histology images of femoral articular cartilage. A-D: surgically induced group. E-H: chemically induced group. Safranin-O/fast green stained with 20x magnification.

Surgically induced group showed apoptosis indicated by empty chondrons (red arrow) during week 4 and superficial fibrillation (red asterisk) during week 8. Chemically induced group showed surface erosion as early as week 8 (red arrowhead).
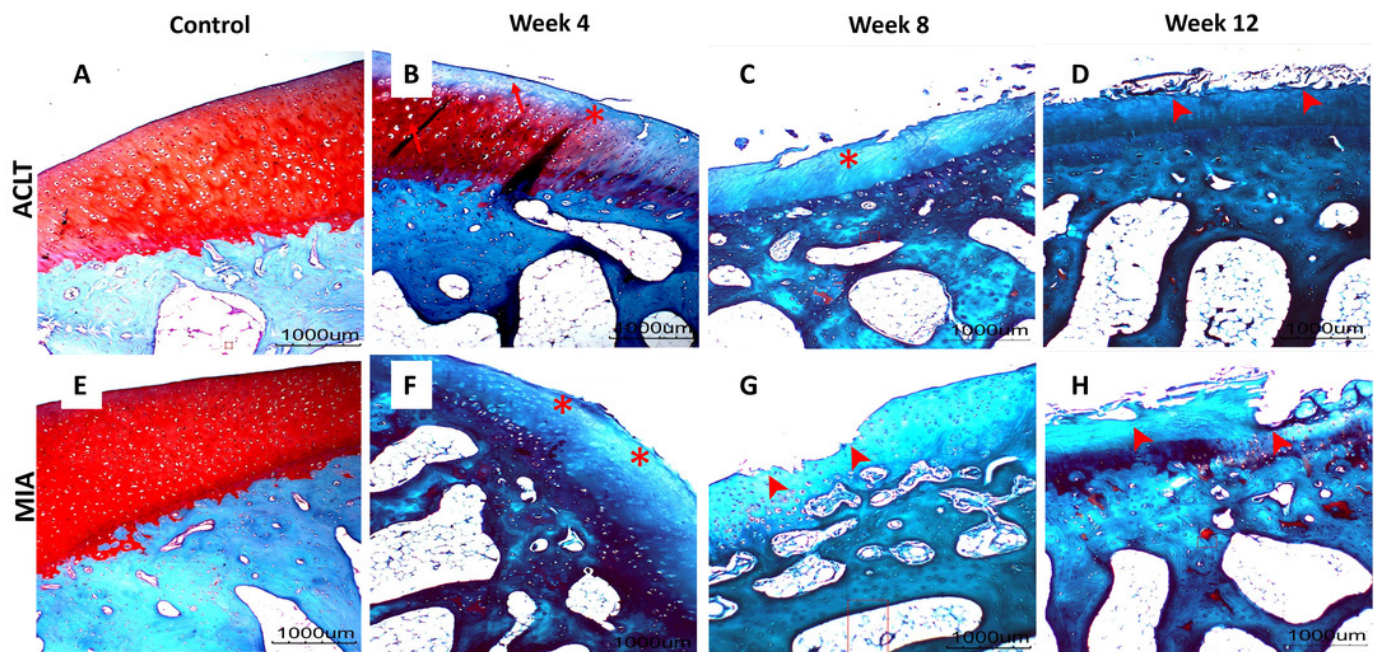
Figure 4

Representative histology images of tibial articular cartilage A-D: surgically induced group. E-H: chemically induced group. Safranin-O/fast green stained with 20x magnification.

During week 4, surgically induced group showed chondrocyte apoptosis (red arrow) and fibrillation (red asterisk) during week 8. Cartilage erosion (red arrowhead) were present during week 12. For chemically induced group, erosion can be observed during week 8 and week 12.
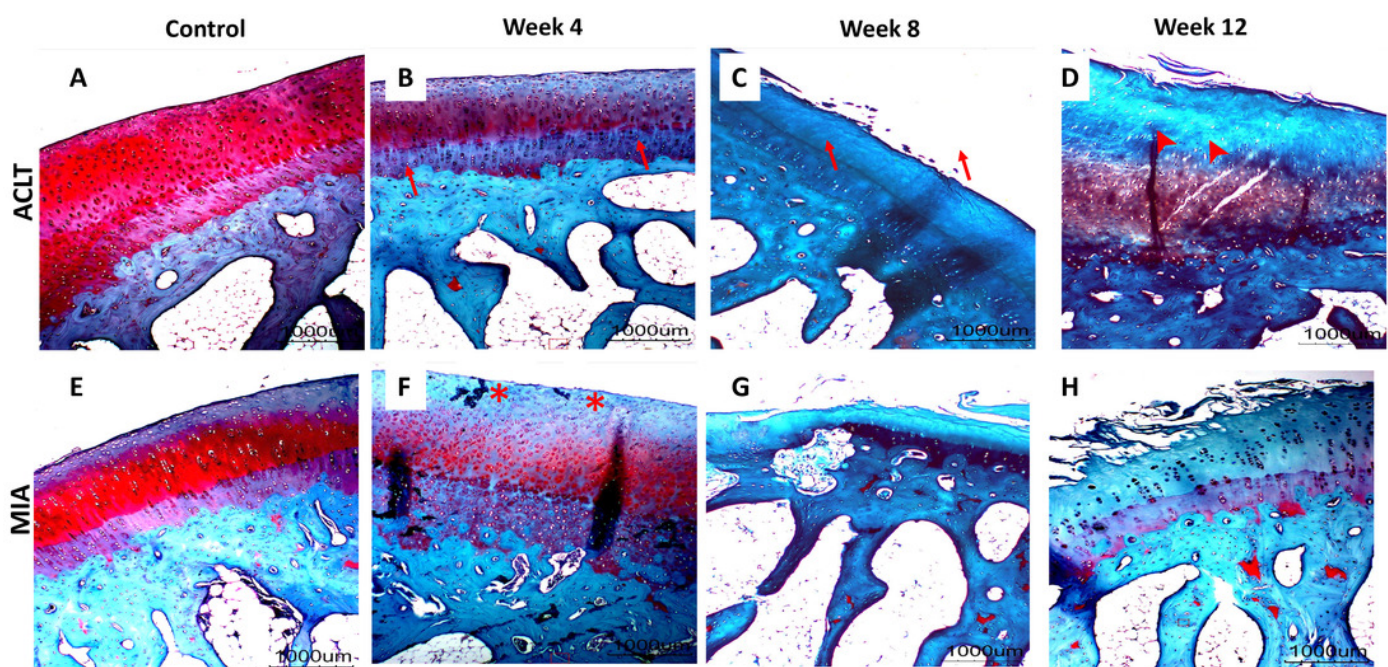
Figure 5

Subchondral bone BV/TV values for (A) femur and (B) tibia in week 4, week 8 and week 12 for the control, surgically (ACLT) and chemically (MIA) induced group.

No significant difference between groups were reported. The results are represented as mean (± SD).
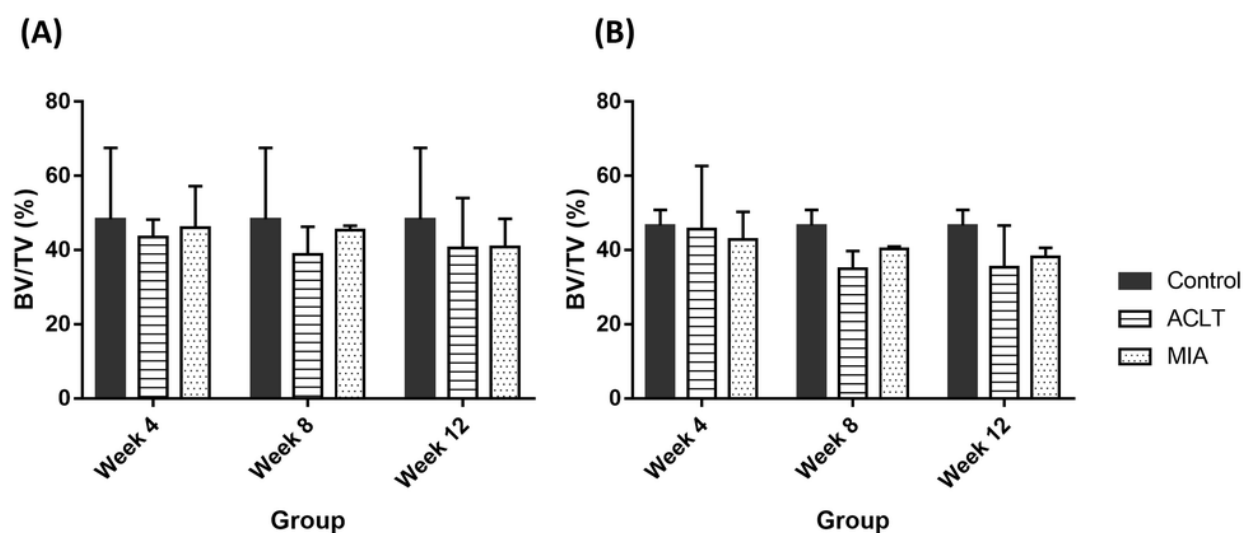
Figure 6

Representative 2DGE (pI 3-10) image for rabbit synovial fluid in (A) surgically induced group and (B) chemically induced group after staining with colloidal Coomassie stain.

Gels from respective groups were scanned and analyzed with Progenesis SameSpot software and protein spots (circled in red) were selected to be picked.